Modelling the rheology of MgO under Earth's mantle pressure, temperature and strain-rates

(final draft post-refereeing)

Patrick Cordier, Jonathan Amodeo & Philippe Carrez

Unité Matériaux et Transformations, UMR 8207 CNRS/Université Lille1, Villeneuve d'Ascq, France

Plate tectonics which shapes the surface of the Earth is the result of solid state convection in the Earth's mantle over billions of years. Simply driven by buoyancy forces, mantle convection is made complicated by the nature of the convecting materials which are not fluids but polycrystalline rocks. Crystalline materials can flow as the result of the motion of defects: point defects, dislocations, grain boundaries, etc. Reproducing in the laboratory the extreme deformation conditions of the mantle is extremely challenging. In particular, experimental strain-rates are at least 6 orders of magnitude larger than in nature[1]. Here we show that the rheology of MgO at pressure, temperature and strain-rates of the mantle is accessible by multiscale numerical modelling, starting from first-principles and with no adjustable parameters. Our results demonstrate that extremely low strain-rates counteract the influence of pressure. In the mantle, MgO deforms in the athermal regime and this leads to a very weak phase. It is only in the lowermost lower mantle that the pressure effect could dominate and that, under the influence of lattice friction, a viscosity of the order of 10^{21}-10^{22} Pa.s can be defined for MgO.

So far, experimental studies dominate the contribution of mineral physics to the study of mantle rheology. Experiments are usually designed to describe how a solid deforms under a constant load (creep tests) or how stress evolves with strain at a constant strain-rate. The on-going challenge is to perform such experiments under pressures representative of the mantle (i.e. up to ca. 135 GPa) and several achievements have been made[2]. The simultaneous determination of the strain rate ($\dot{\varepsilon}$) and of the deviatoric stress (σ) is necessary to parameterize semi-empirical constitutive flow laws $\dot{\varepsilon} = f(\sigma, T, P)$ (often of the power-law form[3, 4]) which are used for extrapolation to natural conditions. A major difficulty is that laboratory strain-rates are of the order of 10^{-6}-10^{-3} s^{-1}, very far from the natural strain rates: 10^{-12}-10^{-16} s^{-1}. Although this issue has been recognized very early[1, 5], it has received very little attention, if any, in the recent years. Here we propose a physically-based model able to describe the rheology of MgO (the magnesium end-member of the second most abundant phase of the lower mantle) under very low strain-rates representative of mantle convection.

All crystalline materials follow the same general evolution with temperature of the critical resolved shear stress (CRSS) for plastic yielding (Fig. 1). At 0K, dislocations move under the influence of stress only. This stress is called the Peierls stress. It measures the intrinsic lattice friction opposed to plastic shear[6]. At finite temperature, dislocation motion is assisted by thermal activation and by stress[7]. A strongly thermally-activated regime is observed (Fig. 1) where plastic shear is governed by the intrinsic mobility of dislocations. A microscopic constitutive equation, called the Orowan equation, describes flow in this regime:

$$\dot{\varepsilon} = \rho b v \qquad (1)$$

where ρ is the mobile dislocation density, b is the Burgers vector modulus and v is the average dislocation velocity. Above a critical temperature T_a (called the athermal temperature) thermal activation is sufficient to overcome lattice friction and plastic shear is essentially athermal, only constrained by dislocations interactions. These fundamental features will be the basis of our model for the rheology of MgO.

In materials science, multiscale modelling has been developed to link our understanding of a few elementary mechanisms (usually at the microscopic scale) with a behaviour observed at the macroscopic scale which might be well characterized but remains poorly understood[8-10]. Concerning plastic deformation, the absence of a global theory results from the range of length- and time-scales spanned. Crystalline plasticity results from the motion of crystal defects: point defects, linear defects (dislocations) or two-dimensional defects (grain boundaries, twin boundaries). Dislocations represent generally the most efficient strain-producing mechanism. Recent calculations[11] have shown that very small grain sizes (100 μm-1mm) would be required for point defect diffusion to dominate the rheology the lower mantle. Moreover, mantle temperatures represent only 40 to 50% of the melting temperature of MgO which is a very refractory oxide. In the present study, we focus on the contribution of dislocation glide on the rheology of MgO.

We have recently proposed a multiscale model of plasticity which combines three modelling ingredients in a logical chain[12]. As described in the Method section, our approach starts with atomistic calculations of dislocation cores which have a paramount influence on dislocation mobility[13]. This mobility is then modelled in the thermally-activated regime using the kink-pairs formalism[14, 15] (see below). Finally, above the

athermal temperature T_a, plastic flow is described within realistic simulations called Dislocation Dynamics[16] (DD). This multiscale approach has been applied to MgO and has shown its efficiency in reproducing the evolution with temperature of the CRSS observed experimentally (Fig. 1). This model is also able of describing the influence of pressure on the plasticity of MgO[17]. In the range of the Earth's mantle, pressure affects the electronic structure and bonding of MgO and has a strong influence on the core structure and mobility of dislocations. This results in an inversion of slip systems from ½<110>{110} to ½<110>{100} under the influence of pressure. Another effect of pressure is to shift T_a toward higher temperatures. At high pressure (and laboratory strain rates) MgO becomes a material characterized by a large lattice friction.

Our physically-based description of the mobility of dislocations gives us the capability of modelling the influence of strain-rate on the rheology of MgO. Overcoming the Peierls energy barrier requires nucleation of a critical bow out (called a kink-pair) on the dislocation line by thermal fluctuations. Rapid lateral motions of the kinks bring the dislocation line into the next low-energy position (Fig. 1). The nucleation rate of kink-pairs is thus generally assumed to limit the dislocation velocity[18]. As a result of this mechanism, the average velocity of a moving dislocation of length L over a Peierls barrier of width a' can be written as[19]:

$$v(\tau,T) = \frac{\nu_D a' b L}{w^2} \exp\left(\frac{-\Delta H_0}{kT}\right) \sinh\left(\frac{\Delta H_0 - \Delta H(\tau)}{kT}\right) \qquad (2)$$

where $\nu_D b/w$ is the vibration frequency for a thermal fluctuation of width w on the dislocation of Burgers vector modulus b and L/w is twice the number of nucleation sites.

This formalism reproduces satisfactorily dislocation dynamics in the thermally activated regime[12, 20, 21]. To extend this formalism to very low stress (or strain-rate) regime : (i) we incorporate explicitly the stress dependence of the kink-pair width $w(\tau)$ and of $\Delta H(\tau)$ as calculated from the kink-pair theory (see Supplementary information), (ii) we take into account possible backward and forward jumps of the kink-pair through the *sinh* function. Figure 2 shows that dislocation velocity curves bend significantly with decreasing stresses (i.e. decreasing strain-rates). A power law based extrapolation (obtained from a linear approximation on a short stress interval in the high-stress regime) to low strain-rates would underpredict the actual velocities.

The rheology of MgO in the thermally-activated regime can be inferred from a combination of equations (1) and (2). The evolution with temperature of the CRSS (available as Supplementary Fig. 4) allows to determine the critical temperature T_a where lattice friction cancels. This is a very important parameter since it represents the frontier between two different deformation regimes. Figure 3 shows that decreasing pressure, like decreasing strain-rate, tends to shift T_a to lower temperatures. At a given temperature and pressure, laboratory and natural strain-rates may induce very different deformation mechanisms. For instance at 60 GPa, 2,000 K, at laboratory strain-rates, MgO deforms on ½<110>{100}, under a CRSS of 215 MPa (due to lattice friction) and with a very non-linear rheology (apparent stress exponent n=13). Decreasing the strain-rate results in a decrease of the stress and of the stress exponent. The second slip system becomes active at ca. 10^{-8} s^{-1} under a stress of 100 MPa. When reaching ca. 10^{-14} s^{-1}, the rheology becomes linear. Below this strain-rate, MgO deforms in the athermal regime where it becomes very plastic and insensitive to temperature and strain-rate.

Mantle conditions[22] are represented on Fig. 3. It appears that in most cases, they correspond for MgO to deformation in the athermal regime which can only be reached at very high-temperatures at laboratory strain-rates. All through the lower mantle, both slip systems ½<110>{110} and ½<110>{100} are activated simultaneously. Figure 4 describes the evolution of the rheology of MgO with mantle depth. Above ca. 2,000 km, MgO deforms in the athermal regime. In this regime, the flow stress is only governed by the dislocation microstructure, it is strain-rate-independent and a viscosity cannot be defined[26]. In this athermal regime MgO appears to be very weak (CRSS below 1 MPa for a dislocation density of 10^8 m^{-2}) and should be much weaker than Mg-silicate perovskite in similar conditions. Below this transition MgO enters a thermally-activated regime. Only there can a viscosity be defined from the Orowan law. We find it of the order of 10^{21}-10^{22} Pa.s with a profile shown on Fig.5. In the vicinity of T_a, the rheology is close to linear and the viscosity is minimum. When the temperature drifts below T_a, the viscosity increases and becomes more strain-rate dependent. Just above the core-mantle boundary, MgO can again enter into a very weak, athermal regime. The depth and extend of this layer characterized by a thermally-activated regime will depend on the thermal state of the lower mantle as illustrated by Fig. 4 which displays several temperature profiles. The actual situation is likely to be even more complex since large thermal heterogeneities (of the order of 1,000 K) are likely to superimpose to these average temperature profiles[26]. Changes of the deformation mechanisms of MgO could thus account for strong radial and lateral rheology heterogeneities inferred in the lowermost mantle[27], even in the absence of significant chemical heterogeneities. However, the sole knowledge of the single crystal rheology of both MgO and Mg-silicate perovskite will not be enough to define the rheology of the mantle. Some form of still larger scale modelling

will be required to bridge from the grain scale to the scale of a cell in a general circulation model of lower mantle dynamics.

METHODS SUMMARY

In this study, we use the hierarchical multiscale approach developed by Amodeo et al.[12] to model the plasticity of MgO single crystals. Atomistic dislocation core structures are modelled with a Peierls-Nabarro-Galerkin (PNG) approach[28]. The electronic structure is explicitly taken into account through γ-surfaces calculated ab initio using VASP[29]. The dislocation mobility, governed by equation (2), is controlled by kink-pairs nucleation. The nucleation enthalpy of kink-pairs $\Delta H(\tau)$ and the kink-pair geometry are evaluated using the Elastic Interaction method[30]. Low stress effects are explicitly taken into account in Eq. 2 by considering the formal geometry of possible backward and forward kink-pair. Mesoscopic scale simulations of MgO deformation processes are performed by DD simulations[16] incorporating dislocation mobilities described by Eq. 2. The accuracy of such multiscale model has been validated against room pressure experimental data[12]. An extended description of the techniques is available in the online-only Methods section.

References

1 Paterson, M.S. Problems in the extrapolation of laboratory rheological data. *Tectonophysics* **133**, 33-43 (1987).

2 Raterron, P. & Merkel, S. In situ rheological measurements at extreme pressure and temperature using synchrotron X-ray diffraction and radiography. *J. Synchrot. Radiat.* **16**, 748-756 (2009).

3 Poirier, J.P. *Creep of crystals* (Cambridge University Press, Cambridge, 1985).

4 Karato, S. *Deformation of Earth Materials: An Introduction to the Rheology of Solid Earth* (Cambridge University Press, Cambridge, 2008).

5 Heard, H.C. Effect of large changes in strain rate in the experimental deformation of Yule marble. *The Journal of Geology* **71**, 162-195 (1963).

6 Peierls, R. The size of a dislocation. *Proc. Phys. Soc. Lond.* **52**, 34-37 (1940).

7 Caillard, D. & Martin, J.L. *Thermally activated mechanisms in crystal plasticity* (Pergamon, Amsterdam, 2003).

8 Bulatov, V.V. & Kubin, L.P. Dislocation modelling at atomistic and mesoscopic scales. *Curr. Opin. Solid State Mat. Sci.* **3**, 558-561 (1998).

9 Needleman, A. Computational mechanics at the mesoscale. *Acta Mater.* **48**, 105-124 (2000).

10 Diaz de la Rubia, T. & Bulatov, V.V. Materials research by means of multiscale computer simulations. *MRS Bulletin* **26**, 169-170 (2001).

11 Ammann, M.W., Brodholt, J.P., Wookey, J. & Dobson, D.P. First-principles constraints on diffusion in lower-mantle minerals and a weak D '' layer. *Nature* **465**, 462-465 (2010).

12 Amodeo, J., Carrez, P., Devincre, B. & Cordier, P. Multiscale modelling of MgO plasticity. *Acta Mater.* **59**, 2291-2301 (2011).

13 Cai, W., Bulatov, V.V., Chang, J., Li, J. & Yip, S. in *Dislocations in solids* (eds Nabarro, F.N.R. & Hirth, J.P.) Vol. 12, 1-80 (Elsevier, Amsterdam, 2004).

14 Seeger, A. & Schiller, P. Bildung und Diffusion von Kinken als Grundprozess der Versetzungsbewegung bei der Messung der inneren Reibung. *Acta Metall.* **10**, 348-357 (1962).

15 Guyot, P. & Dorn, J.E. A critical review of Peierls mechanism. *Can. J. Phys.* **45**, 983-1015 (1967).

16 Devincre, B., Kubin, L.P., Lemarchand, C. & Madec, R. Mesoscopic simulations of plastic deformation. *Mater. Sci. Eng. A* **309**, 211-219 (2001).

17 Amodeo, J., Carrez, P. & Cordier, P. Modeling the effect of pressure on the critical shear stress of MgO single crystals. *Phil. Mag.* (Submitted).

18 Frost, H.J. & Ashby, M.F. *Deformation-mechanism maps : the plasticity and creep of metals and ceramics* (Pergamon Press, Oxford, 1982).

19 Nabarro, F.R.N. One-dimensional models of thermal activation under shear stress. *Phil. Mag.* **83**, 3047-3054 (2003).

20 Tang, M., Kubin, L.P. & Canova, G.R. Dislocation mobility and the mechanical response of bcc crystals: a mesoscopic approach. *Acta Mater.* **46**, 3221-3235 (1998).

21 Monnet, G., Devincre, B. & Kubin, L.P. Dislocation study of prismatic slip systems and their interactions in hexagonal close packed metals: application to zirconium. *Acta Mater.* **52**, 4317-4328 (2004).

22 Ono, S. Experimental constraints on the temperature profile in the lower mantle. *Phys. Earth Planet. Inter.* **170**, 267-273 (2008).

23 Anderson, O.L. The Earth's core and the phase diagram of iron. *Philos. Trans. R. Soc. London A* **306**, 21–35 (1982).

24 Brown, J.M. & Shankland, T.J. Thermodynamic parameters in the Earth as determined from seismic profiles. *Geophys. J. R. Astron. Soc.* **66**, 579–596 (1981).

25 Schuberth, B.S.A., Bunge, H.-P., Steinle-Neumann, G., Moder, C. & Oeser, J. Thermal versus elastic heterogeneity in high-resolution mantle circulation models with pyrolite composition: High plume excess temperatures in the lowermost mantle. *Geochem. Geophys. Geosyst.* **10**, Q01W01 (2009).

26 Paterson, M.S. Relating experimental and geological rheology. *Int. J. Earth Sci.* **90**, 157-167 (2001).

27 Forte, A.M. & Mitrovica, J.X. Deep-mantle high-viscosity flow and thermochemical structure inferred from seismic and geodynamic data. *Nature* **410**, 1049-1056 (2001).

28 Denoual, C. Dynamic dislocation modeling by combining Peierls Nabarro and Galerkin methods. *Phys. Rev. B* **70**, 024106 (2004).

29 Kresse, G. & Hafner, J. Ab initio molecular-dynamics for liquid-metals. *Phys. Rev. B* **47**, 558-561 (1993).

30 Koizumi, H., Kirchner, H.O.K. & Suzuki, T. Kink pair nucleation and critical shear-stress. *Acta Metall. Mater.* **41**, 3483-3493 (1993).

Supplementary Information is linked to the online version of the paper.

Acknowledgements This work was supported by ANR (Diup project).

Author Contributions P.C. conceived the project. P.C. and Ph.C. designed the work. J.A. and Ph.C. performed numerical simulations. All authors discussed and interpreted the results. P.C. wrote the paper with feedback and contributions of all co-authors.

Author Information The authors declare no competing financial interests.

Correspondence and requests for materials should be addressed to P.C. (Patrick.Cordier@univ-lille1.fr).

Figures

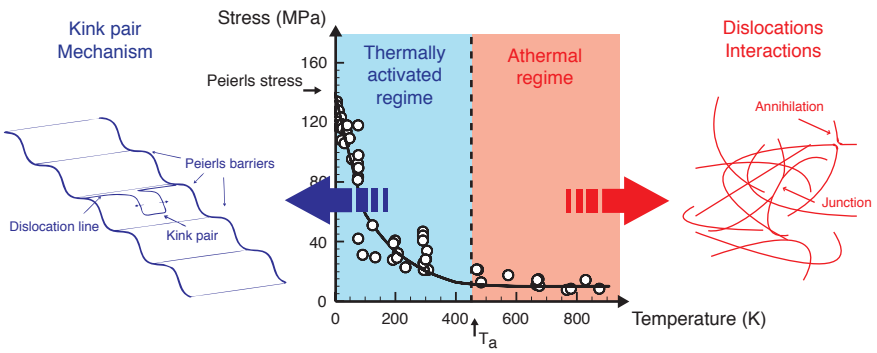

Figure 1: Evolution of the critical resolved shear stress (CRSS) with temperature. Following the Peierls stress at 0 K, the CRSS is strongly temperature dependent until the athermal temperature T_a is reached. Below T_a, lattice friction dominates and plastic flow is controlled by the mobility of dislocations governed by the kink-pair mechanism. Above T_a, plastic flow is essentially athermal (plateau) and dislocation interactions dominate. In the central panel, this general behaviour is illustrated for ½<110>{110} glide in MgO at ambient pressure. Symbols refer to experimental data (see Supplementary Information for more details) and the line corresponds to our model[12].

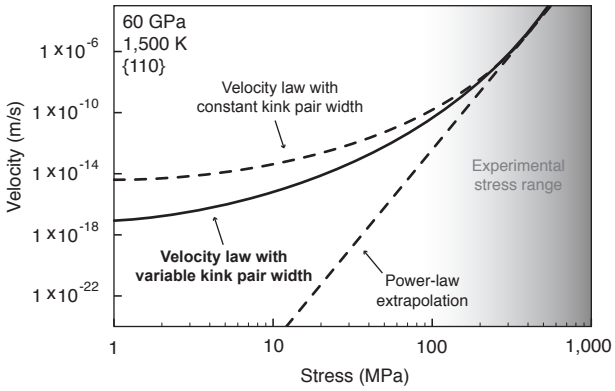

Figure 2: Evolution with stress of the velocity of a ½<110> screw dislocation gliding in {110} at 60 GPa, 1,500 K. The effect of incorporating variable kink-pair width in Eq. 2 is shown on the bending of the curve. As a result, the stress dependence does not obey a power law on a wide stress interval. Extrapolation of laboratory data to very low strain-rates (corresponding to low stresses) based on a power law fitted against high-stress data is thus invalid.

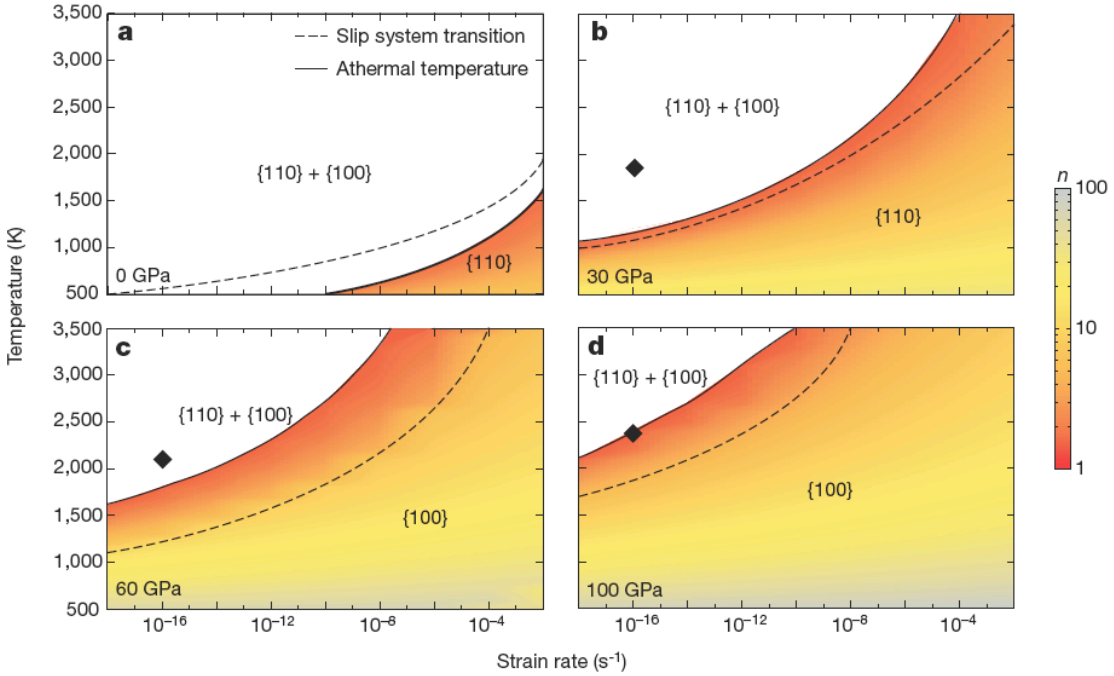

Figure 3: Influence of the strain-rate on the deformation mechanisms of MgO. **a** 0 GPa, **b** 30 GPa, **c** 60 GPa and **d** 100 GPa. The line between the white and coloured regions corresponds to the athermal temperature T_a. In the thermally-activated domain (coloured) we have calculated and represented an apparent stress exponent. The dotted line separates domains where different slip systems dominate. The dominant glide planes are featured. The diamond symbol represents average mantle conditions corresponding to these pressures[22].

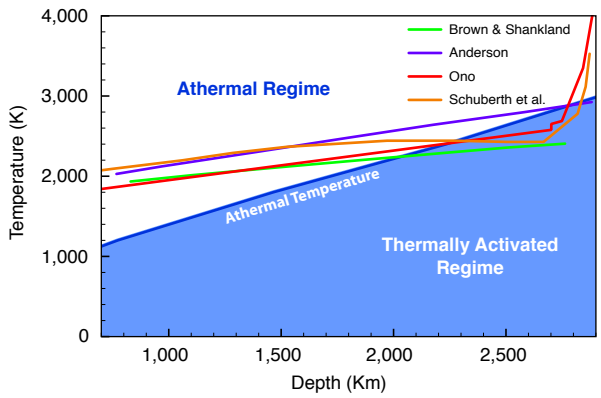

Figure 4: Deformation mechanisms of MgO under mantle conditions (and a typical strain rate of 10^{-16} s^{-1}). The athermal temperature is compared to several geotherms[22-25]. The exact interval where MgO deforms in the thermally activated regime depends on the thermal state of the mantle and, given lateral thermal heterogeneities[25], can vary significantly from place to place.

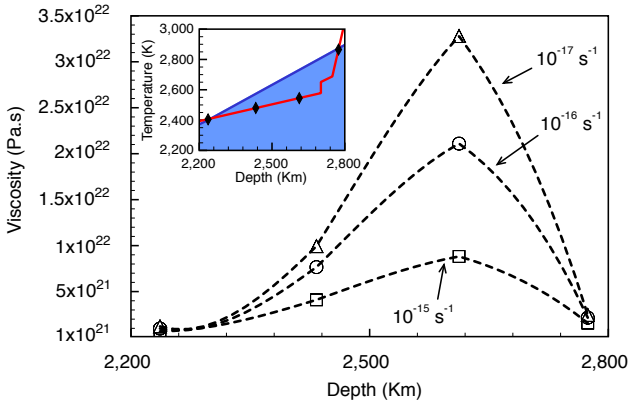

Figure 5: MgO viscosity profile in the layer governed by the thermally-activated deformation regime. The depth interval between 2,200 and 2,800 km corresponding to the geotherm of Ono[22] within Fig. 4 is reproduced in the insert. The symbols along the geotherm (in red) correspond to the viscosity calculations. The dotted line are just guide for the eyes. It is to be noted that since decreasing the strain-rate by an order of magnitude results in a very small variation of the stress, the viscosity increase when the strain-rate decreases. The more the temperature drifts apart from T_a, the more pronounced this non-linearity becomes.

METHODS

The hierarchical multi-scale model used throughout this study, has been initially developed by Amodeo et al.[12] and applied to pure MgO single crystals. It connects modelling at three different scales. The first one corresponds to the modelling of dislocation core structures and associated Peierls stresses (the stress required to move a dislocation without the help of thermal activation). The second stage incorporates the temperature effect on intrinsic dislocation mobility. The last stage describes dislocation interactions and yields single crystal mechanical properties.

Peierls-Nabarro Galerkin modelling of dislocation cores. Peierls-Nabarro (PN) methods[6] and their recent developments[28,31,32] based on γ-surfaces, are very efficient to model dislocation core structures[33]. Here we use the Peierls-Nabarro-Galerkin model[28,34] as implemented in the Cod²*ex* software which offers the possibility to take multiple glide planes into account and to calculate complex (possibly three-dimensional) dislocation cores. As in the initial PN model, the dislocation core structure is determined from the minimization of an elastic energy (through an approximation of a continuous field representation) and an interplanar potential derived from γ-surfaces calculations. The present study uses pressure-dependent γ-surfaces calculated from first principles. Indeed, the pressure range of the Earth's lower mantle rules out the use of empirical potentials and justifies the use of Density Functional Theory (DFT) calculations, which are believed to be more accurate.

Classical DFT approximations (namely GGA with PAW pseudo-potentials[35-37], as implemented in the VASP code[29,38]) have been used to calculate the excess energy

associated with a rigid-body shear of a supercell along a given plane (corresponding to the strict definition of a γ-surface[39]). Three different γ-surfaces, namely {110}, {100} and {111}, have been considered. As a consequence, three distinct supercells have been built for VASP calculations. Supercells are built on a Cartesian reference frame with the *z* axis normal to the shear plane. In order to reduce the number of atoms in each supercell, the *x* and *y* directions are chosen according to shortest crystallographic directions, i.e. ½<110> and <001> for the {110} supercell, two perpendicular ½<110> directions for the {100} supercell, and ½<110> and ½<112> for the {111} supercell. Doing so, the supercells contain a minimum of 16 atomic layers with a single stacking fault plane located in the middle of the supercell, isolated from periodic boundary replica by a buffer of a minimum of 6 Å-thick vacuum layer. A Monkhorst-Pack grid[40] is used to sample first Brillouin zone with a grid points number increased to 6x4x2 for convergence energy purpose. Calculations have been performed at 0, 30, 60 and 100 GPa.

Both edge and screw dislocation cores have been calculated through the PNG method. In this approach, two distinct fields are used to minimise the energy of a system in which an initial Volterra dislocation has been introduced. One is a three-dimensional displacement field which represents the continuous deformation around the dislocation core whereas the second is a vector field which represents the displacement jump when crossing discontinuity surfaces characterized by γ-surfaces. Minimization with respect to the vector field is achieved by means of a time-dependent Ginzburg-Landau equation whereas an element free Galerkin method is used to compute the evolution of the three-dimensional displacement field.

PNG finite-element cells are defined with a node structure reflecting the crystalline symmetry of the crystal. A classical node density of 12 nodes per Burgers vector was chosen for all the calculations. For screw dislocation calculations, four families of planes are considered to control the spreading of shear within the core, namely $(1\bar{1}0)$, (001), $(1\bar{1}1)$ and $(1\bar{1}\bar{1})$. Between those planes (associated with γ-surfaces), the medium exhibits a linear elastic behaviour. The method ensures that potentially non-planar core dislocations can be safely reproduced. Once the equilibrium configuration of the dislocation core is reached, the PNG finite elements cell can be strained in order to determine the Peierls stress, for which a dislocation displacement is irreversible in its glide plane.

Kink-pair model. In presence of lattice friction, dislocation motion is thermally activated[13]. Practically, a dislocation line moves from one Peierls valley (corresponding to a minimum energy position) to the next, through the nucleation and propagation of kink pairs[7,41]. Several methods[7] exist to model the kink-pair mechanism; among them are the Line Tension (*LT*) and Elastic Interaction (*EI*) models[14,30]. The *EI* method has been chosen in this study since it is commonly regarded as a low-stress model[7]. It gives access to the stress dependence of the formation enthalpy for critical kink-pairs configurations.

The rate of kink-pair nucleation is thermodynamically controlled by the free energy required to displace a critical dislocation segment into the next Peierls valley. When neglecting the associated entropy[42], this energy can be approximated to the activation enthalpy ΔH. Within the *EI* assumptions, ΔH results from three contributions: the elastic interaction energy ΔE, the variation of the Peierls energy ΔP between a straight line and

a kinked one and W, the work of the applied stress τ. Assuming a rectangular shape for the kink-pair configuration of height h and width w, the variation of enthalpy takes the following form:

$$\Delta H(h,w) = \Delta E(h,w)+\Delta P(h,w)-W(h,w) \quad (3)$$

A critical shape (h^*,w^*) of the bow out configuration and the associated critical enthalpy ΔH^* can thus be calculated in the saddle point configuration as a function of stress τ. Considering a rectangular kink pair, we use the expression of ΔE proposed by Hirth & Lothe[41] in which the self-energy of dislocation is controlled by a cut-off length. In this study, this cut-off length is parameterized on the half-width of dislocation core (accessible from the previous stage of modelling). Half-width of dislocation cores, core structures and Peierls stresses τ_p calculated by the PNG method are also used to define the Peierls potential V_P controlling the numerical evaluation of ΔP[30]. Therefore, this formalism is closely related and linked to the atomic scale information previously calculated.

Dislocation Dynamics (DD) simulations have been performed using the open source simulation package mM[16,21]. It corresponds to a discrete three-dimensional dislocations dynamics code accounting for complex boundary conditions. Here, periodic boundary conditions are used in the calculations to model plasticity in bulk conditions[43]. DD simulations with the mM code are also known as discrete dislocation dynamics simulations as they rely on a discretization of both space and time. For a given slip system geometry, dislocation lines are discretized into a finite set of segments of fixed characters, screw, edge and mixed. Straight, glissile segments, are therefore moved on a

3D lattice exhibiting the lattice symmetry of the simulated crystal structure. For MgO, the underlying lattice is thus composed of 96 elementary segments belonging to 12 possible slip planes in order to satisfy for the two possible slip systems families, ½<110>{110} and ½<110>{100}.

The long-range interactions are treated through Peach-Koehler forces. Besides the applied stress specific of loading conditions, stress acting on discretized segments takes into account the stress field associated with the whole set of dislocation lines present in the simulated volume, plus the line tension. During deformation, local rules are prescribed to account for contact reactions, such as annihilations or junctions formation[44]. Finally, throughout the thermally activated regime, discrete dislocation segments move with a velocity law described by Eq. (2). The method assumes that kink-pair nucleation is the controlling stage and relies on numerical key parameters coming from the two previous step of the modelling scheme.

Series of compression test simulations at various temperatures are used to determine the CRSS of MgO. To that purpose, one may undertake DD simulations at a constant strain rate using an initial straight dislocations (of either screw or edge character depending on the pressure-temperature range investigated) distribution of characteristic lengths $1/\sqrt{\rho}$ of 100 μm in a simulated volume. Dislocation lines are initially along a diagonal of the basis plane of the simulated volume which is parallel to {001}, so that identical simulations conditions can be used to promote glide in either {100} or {110} planes by simply varying the compression axis.

References

31 Joos, B., Ren, Q. & Duesbery, M.S. Peierls-Nabarro model of dislocations in silicon with generalized stacking-fault restoring forces. *Phys. Rev. B* **50**, 5890-5898 (1994).

32 Bulatov, V.V. & Kaxiras, E. Semidiscrete Variational Peierls Framework for Dislocation Core Properties. *Phys. Rev. Lett.* **78**, 4221-4224 (1997).

33 Schoeck, G. The core structure of dislocations: Peierls model vs. atomic calculations. *Acta Mater.* **54**, 4865-4870 (2006).

34 Denoual, C. Modeling dislocation by coupling Peierls-Nabarro and element-free Galerkin methods. *Comp. Methods Appl. Mech. Eng.* **196**, 1915-1923 (2007).

35 Perdew, J.P. & Wang, Y. Accurate and simple analytic representation of the electron-gas correlation energy. *Phys. Rev. B* **45**, 13244-13249 (1992).

36 Blöchl, P.E. Projector augmented-wave method. *Phys. Rev. B* **50**, 17953-17979 (1994).

37 Kresse, G. & Furthmüller, J. Efficiency of ab-initio total energy calculations for metals and semiconductors using a plane-wave basis set. *Comput. Mat. Sci.* **6**, 15-50 (1996).

38 Kresse, G. & Hafner, J. Ab initio molecular dynamics simulation of the liquid-metal amorphous-semiconductor transition in germanium. *Phys. Rev. B* **49**, 14251 (1994).

39 Vítek, V. Intrinsic stacking faults in body-centered cubic crystals. *Phil. Mag.* **18**, 773-786 (1968).

40 Monkhorst, H.J. & Pack, J.D. On special points for Brillouin-zone integrations. *Phys. Rev. B* **13**, 5188 (1976).

41 Hirth, J.P. & Lothe, J. *Theory of dislocations*. (John Wiley & Sons, Inc, New York, 1982).

42 Schoeck, G. The activation energy of dislocation movement. *Phys. Stat. Sol.* **8**, 499-507 (1965).

43 Madec, R., Devincre, B. & Kubin, L.P. in *IUTAM Symposium on Mesoscopic Dynamics of Fracture Process and Materials Strength* (eds Koizumi, H. & Yip, S.) 35-44 (Kluwer Academic Publishers, NL-Dordrecht, 2004).

44 Kubin, L.P., Madec, R. & Devincre, R. Dislocation Intersections and Reactions in FCC and BCC Crystals. *Materials Research Society Symposium Proceedings* **779**, 25-36 (2003).